https://doi.org/10.5194/os-2020-58
Preprint. Discussion started: 18 June 2020

Ocean Science
Discussions
Open Access
EGU

Coastal mesoscale processes and their effect in phytoplankton distribution and community composition in the SE Bay of Biscay

Xabier Davila[1], Anna Rubio[1], Felipe Artigas[2], Ingrid Puillat[3], Ivan Manso-Narvarte[1], Pascal Lazure[3], and Ainhoa Caballero[1]

[1]AZTI-Tecnalia, Marine Research Division, Herrera kaia portualdea z/g, 20110 Pasaia, Spain
[2]Université du LIttoral Côte d'Opale, Université de Lille, CNRS UMR 8187 LOG, Wimereux, France.
[3]IFREMER/Dyneco/Physed, BP 70, 29280 Plouzané, France.

Correspondence: Xabier Davila (Xabier.Davila@uib.no)

Abstract.

Mesoscale dynamics have a determinant role in several ocean processes, not only in the transport of momentum, heat, mass and particles but also in the provisioning of nutrients into the euphotic zone. Mesoscale processes can define niches where specific phytoplankton species flourish. However, this effect is not straightforward in coastal areas, which are submitted to a more complex interplay between different oceanic processes. In this context, the ETOILE campaign surveyed the CapBreton canyon area in the South-East of Bay of Biscay in early August 2017. The main objective of this study was to link the occurrence and distribution of phytoplankton with the mesoscale ocean processes. On top of the remote sensing data available for this area, such as High Frequency radar or satellite data, in situ discrete hydrographic measurements were carried out by a CTD and a Moving Vessel Profiler. Likewise, multi-spectral fluorescence casts were performed in selected stations. Other parameters such as temperature, conductivity and in vivo multi-spectral fluorescence were also continuously recorded at surface. From our observations, we discuss on the distinct effect and importance of different factors affecting the phytoplankton distribution. Overall, salinity is the most important parameter modulating not only algae distribution but also the composition of the community in terms of spectral groups. Although below the mixed layer salinity still impacts significantly phytoplankton, vorticity comes into play and becomes the dominant factor determining both distribution and composition. The present study brings into consideration the relevance of the dynamic variables in the study of phytoplankton, despite targeting only hydrographic variables.

1 Introduction

The monitoring and characterization of mesoscale dynamics is determinant for the appropriate comprehension of marine ecosystems. One the main factors modulating the ecosystem functioning, primary production, is crucially dependant on the transport of limiting nutrients to the sunlit surface ocean. Although mesoscale events are confined in time and space, the time at which they evolve and transport seawater properties -i.e nutrients- is similar to the phytoplankton growth timescales (Mahadevan, 2016). The production of organic matter from inorganic nutrients and carbon through photosynthesis also affects the ocean's carbon storage and its ability to regulate atmospheric carbon dioxide. Hence, eddies might actively contribute to the

https://doi.org/10.5194/os-2020-58
Preprint. Discussion started: 18 June 2020

carbon export and regulate the fate of particulate organic carbon and the regions' biogeochemical budgets (Mahadevan, 2014). Even if it is known to affect the distribution of surface and subsurface chlorophyll rich waters in the South-Eastern sector of Bay of Biscay (SE-BoB), in coastal areas the eddies interact with complex ocean dynamics and thus this link is not so straightforward (Caballero et al., 2016; Rubio et al., 2018). In addition, this cross-shelf transport has also implication in fields such as plankton studies, fisheries and management, as it transports a wide variety of "particles", such as phytoplankton, zooplankton and fish egg or larvae (Irigoien et al., 2007).

The BoB is a semi-open bay limited by the Spanish coast in the southern part and the French coast in the eastern part. South of Cape Breton, the Cantabrian shelf is 10 km narrow, while to the north, the French shelf becomes wider, reaching 150 km width in the Aquitaine coast. The ocean surface layer in this region is subjected to the seasonal variations the water runoff from nearby rivers Gironde, Loire and Adour (Reverdin et al., 2013). The runoff occurs mainly from winter to spring and it significantly modifies the water mass adjacent to the shelf (Caballero et al., 2016) creating turbid and dilution plumes, known as Regions of Freshwater Influence (ROFI) (Sharples and Simpson, 1993). During winter, the runoff water mixes with the coastal oceanic water and forms a frontal zone of intermediate salinity in the shelf break (Puillat et al., 2006). As the freshwater surface layer warms up in spring, it isolates from the bottom by a colder layer left from the previous winter water (Reverdin et al., 2013). The river discharge acts as a nutrient source to the surface layers that sustains primary production in the region (Morozov et al., 2013).

The circulation in this area is complex and controlled mainly by the prevailing winds, on a wide range of timescales from seasonal variations to high frequency processes associated with breezes (Solabarrieta et al., 2014). Although the general circulation pattern in the area is characterised by a weak anticyclonic circulation in the central region (Figure 1), coastal areas are much more dependent on wind conditions (Valencia et al., 2004; Pingree and Garcia-Soto, 2014). During autumn and winter, winds are mostly south-westerly, driving northern and eastern drift over the shelf. On the contrary, in spring and summer the prevailing north-easterly wind results in west-southwest flow of the currents (Solabarrieta et al., 2014). This wind pattern either reinforces or weakens the existing slope current, also known as the Iberian Poleward Current (IPC). Being a branch of the Azores current, during autumn and winter, the IPC advects warm and saline water poleward, flowing eastwards in the Cantabrian shelf. On the contrary, during spring and summer this current weakens and even reverse, flowing southwards in the French shelf, and westwards in the Spanish shelf (Rubio et al., 2013). When the IPC interacts with the abrupt bathymetry the generated instabilities develop into Slope Water Oceanic eDDIES (SWODDIES) (Caballero et al., 2016). These have been extensively studied (Caballero et al., 2014, 2016; Ferrer and Caballero, 2011; Garcia-Soto, 2002), mainly via satellite data due to their surface signal recorded in Sea Surface Temperature (SST), Chlorophyll-a (Chl-a) and altimeter, as well as with in situ data. More recently, and since the installation of High Frequency Radar (hereinafter HF radar) in the South Eastern BoB, Rubio et al. (2018) analysed the surface water velocities of these SWODDIES.

https://doi.org/10.5194/os-2020-58
Preprint. Discussion started: 18 June 2020

Few studies provide the link between phytoplankton occurrence and physical processes in the BoB. Fernández et al. (1993) described how the flow of the IPC over the Cantabrian shelf generates a shelf-break convergent front that separates the advected high-salinity and warm waters from the cold fresher coastal waters. The vertical mixing associated to this frontal system had a substantial influence on the whole planktonic community. More recently, Caballero et al. (2016) reported a Deep Chlorophyll Maximum (hereinafter DCM) in the centre of a SWODDIE induced by mesoscale eddy dynamics. This resulted from a combination of quasi-geostrophic vertical velocities and eddy-wind induced Ekman pumping in the centre of the anticyclone. Although not in the BoB, D'Ovidio et al. (2010) linked the different groups phytoplankton with the surface ocean dynamics by combining the use of a numerical algorithm called PHYSAT and altimetry data. They defined the so-called fluid dynamical niches where the phytoplankton assemblages interact with distinct physiochemical environments, such as eddies. However, this approach is only available for mesoscale to large scales dynamics due to the resolution of satellite products.

In order to the shed light on the coastal mesoscale dynamics and its effects on phytoplankton distribution in the most inner part of BoB, the ETOILE campaign surveyed the Capbretron Canyon area on early August 2017. In this campaign, various hydrographic and hydrodynamic data were collected and compared to different phytoplankton pigmentary groups addressed by multi-spectral fluorometry. The ETOILE campaign was part of different efforts that have been carried out recently in the framework of JERICO-NEXT (H2020) European project, partially focused on the quantification of the potential impact of the ocean transport on the distribution of plankton or other pelagic organisms in line with several MFSD main descriptors. Both JERICO-NEXT (2014 - on going) and its predecesor JERICO (2007–2013) assist on the improvement and creation of coastal observatory networks as well as the applications of these for addressing European marine policies. Here we describe the mesoscale processes that are present in the area of CapBreton canyon and we link the different hydrographic and hydrodynamic variables to the occurrence and distribution of two main different pigmentary groups of phytoplankton, brown and green algae.

2 Material and Methods

2.1 ETOILE Campaign

In the framework of the European H2020 Joint European Research Infrastructure for Coastal Observatory - Novel European eXpertise for coastal observaTories (JERICO-NEXT) project, the "Côtes de la Manche" research vessel (CNRS-INSU), surveyed the area of CapBreton canyon from the 2nd to the 4th of August 2017 during the Leg 2.2 of the ETOILE oceanographic campaign (P.I. Pascal Lazure, IFREMER, DOI: 10.17600/17010800), aiming to undercover the mesoscale dynamics. The campaign consisted in six transects covering the continental shelf and slope, as well as the axis of the canyon, as showed in Figure 2. During east-west transects (T1, T3 and T5) a CTD (Sea-Bird) was deployed every 7 km, while during west-east (from offshore to onshore) transects a Mobil Vessel Profiler (MVP200 operated by Genavir) was towed.

https://doi.org/10.5194/os-2020-58
Preprint. Discussion started: 18 June 2020

During the campaign chlorophyll was estimated by a FluoroProbe (bbe Moldakenke) multi-spectral fluorometer, which measures fluorescence emission of chlorophyll after excitation through accessory pigments using LEDs with different wavebands. It makes it possible to differentiate up to four algal pigmentary groups: "blue algae" (mainly corresponding to Cyanobacteria), "green algae" (mainly Chrolorophytes but also Crysophytes, Prasinophytes and to some extent Haptophytes; Houliez et al., 2012), "brown algae" (mainly diatioms, part of the dinoflagellates, part of the Haptophytes) and "mixed group" (Cyanobacteria, Cryoyptophytes, some Dinoflagellates). It estimates chlorophyll-a (chl-a) equivalent concentrations for these four groups (as well as total chl-a) and also provides an estimation of the concentration of chromophoric dissolved organic matter (CDOM or yellow substances). Up to 80 m depth in vivo fluorescence profiles were obtained. Unfortunately, this data could just be gathered in the T3 and T5 transects due to technical issues with the instrument during T1. During the whole campaign salinity and in vivo fluorescence were continuously measured on surface (3.5 m deep) by a thermosalinograph and a second automated multi-spectral fluorometer, respectively. Due to an instrumental bias and different measuring sensitivity, this data was excluded from the posterior quantification. However, this continuous record at surface provided a valuable qualitative information, since the resolution of satellite data is too low at the near-submesoscale.

2.2 Complementary operational remote sensing data

In addition to the in-situ data, remote sensing operational data was used to complete the picture obtained during ETOILE. Ocean surface currents measurements were obtained by two long-range HF radar antenna located at Matxitxako and Higer Cape and owned by the Directorate of Emergency Attention and Meteorology of the Basque Security Department. They emit at a central frequency of 4.463 MHz and a 30-kHz bandwidth which integrates vertically the horizontal velocities in the first 1.5 m of the water column (Rubio et al., 2013). The receiving signal, an averaged Doppler backscatter spectrum, allows to estimate surface currents over wide areas (reaching distances over 100 km from the coast) with high spatial (1-5 km) and temporal ($\leq$1 h) resolution (Figure 2 lower left corner). In order to obtain the surface velocity data we followed the methodology of Rubio et al. (2013). Velocity data is processed from the spectra of the received echoes every 20 minutes using the MUSIC (MUltiple SIgnal Classification) algorithm. Then, a centred 3h running mean average was applied to the resulting radial velocity fields.

For this study, in order to visualize representative velocity fields we applied a low-pass 10th order digital Butterworth low-pass filter (Emery and Thomson, 2001) to both of the velocity components at each node (filtering out T$<$48 h). Therefore, HF processes such inertial currents or tides were removed, as these are irrelevant for the purposes of this study and would have eclipsed the mesoscale geostrophic and synoptic wind circulation patterns. Likewise, a Lagrangian Particle-Tracking Model (LPTM) was applied to HF radar data to simulate the observed trajectories. Particles released within the HF radar coverage area are advected, at a low computational cost. The method used for the particle movement in this LPTM is based upon the 4th order Runge–Kutta scheme (Benson, 1992). In this case, the particles are advected using the 2D hourly current fields given by the HF radar. To describe mesoscale patterns, Lagrangian Residual Currents (LRC) were calculated following a methodology

https://doi.org/10.5194/os-2020-58
Preprint. Discussion started: 18 June 2020

similar to that described in (Muller et al., 2009), using an integration time of 3 days.

Furthermore, satellite data prior and after the campaign was also analysed. SST and Chlorophyll-a data was retrieved from the Visible and Infrared Imager/Radiometer Suite (VIIRS) sensor and water turbidity, from MODIS. In addition to these datasets, hourly wind information of July and August was collected by the mooring buoy of Bilbao owned by "Puertos del Estado" (available in www.puertos.es). Although its location is not exactly on our study area (Figure 2) it is considered close enough for a general description of the wind regime in the bay.

2.3 Computation of vorticity and vertical velocities

From hydrographic data alone, geostrophic circulation can be diagnosed, inferring various key dynamical variables such as geostrophic relative vorticity (hereinafter referred to just as vorticity) or the vertical velocity from a 3D snapshot of the density field. To compute vertical velocities, we assume quasi-geostrophic dynamics and a synoptic or steady state, where the Rossby number is small and mesoscale features remain constant during the sampling (Gomis et al., 2001). As the time/space distribution of the observations are important, the use of the Moving Vessel Profiler (hereinafter MVP) allowed a more extensive and quicker sampling suitable for small, rapidly evolving structures. In order to reduce the computational effort during the analysis of the data, the MVP transects were averaged every 5 km, considering it enough resolution or resolving (sub)mesoscale structures, following the methodology in Gomis et al. (2001). An interpolation of the data allows to derive those key dynamical variables and get a high-resolution image of the (sub)mesoscale dynamics. This was accomplished by merging the CTD and averaged MVP profiles after verifying that no significant bias was present between the measurements of these two instruments. Once having verified that data can be merged, the Optimal Statistical Interpolation (OSI) was performed by the 'DAToBJETIVO' software package developed by Gomis and Ruiz (2003), for the objective spatial analysis and the diagnosis of oceanographic variables.

For the interpolation in the sampling area a 11 x 33 output grid was used with a 0.031° x 0.033° resolution (Figure 2), pursuing a compromise between providing a good representation of the scales that are able to be resolved by the sampling and minimizing the effect of the observational error. This resulted in a coarse grid that allowed the correct representation of the subsequent spatial derivatives of the analysed field Gomis et al. (2001). In the vertical, 98 equally-spaced levels were considered, from 4 to 200 m (every 2 m). In order to analyse and correlate the explanatory and the response variables, the same interpolation was performed for the fluorescence data.

Once calculated the whole set of hydrographic and dynamic variables that describe the ocean physical environment, we can compare them to fluorescence data, sharing a common grid. Two approaches were followed in order to understand the factors involved in the phytoplankton distribution. First we employed a set of General Additive Models (GAMs; Hastie and Tibshirani (1990) for a first understanding of the covariance between the explanatory variables and phytoplankton. GAMs

https://doi.org/10.5194/os-2020-58
Preprint. Discussion started: 18 June 2020

offer the possibilities of identifying non-linear relationship between variables by the inclusion of a smoothing function that has no specific shape. These are a powerful tool for data exploration and have been successfully used for the spatial analysis of phytoplankton (Llope et al., 2009, 2012). The presented GAMs were carried out by the R package "mgcv" (Wood, 2011). In addition to the GAM analysis, and after identifying the key responses to be linear, we proceeded to what we think is a better approach to disentangle the relative importance of each factor. We divided our dataset in progressively smaller subsets in relation with the fluorescence and then use a linear regression to understand the main modulating factor in each of the subsets.

3 Results

3.1 Mapping coastal mesoscale hydrography and currents

In order to understand the hydrodynamic context in which the campaign took place, it was mandatory to determine the wind conditions. As mentioned before, wind intensity and direction play a major role in determining the surface oceanographic setting in the SE-BoB. Figure 3 shows the Progressive Vector Diagram (PVD) of the wind conditions. From the 21^{st} to the 28^{th} of July, the predominant wind had a marked north-westerly component with relatively high intensity. Then, it decreased in intensity and reverse and started blowing from the north-east. The 7^{th} of August the wind had again a north-west component for few days. The wind conditions during the whole campaign remained relaxed, variable in direction but low in intensity.

The combined use of wind data and satellite imagery together with the HF radar provide a context of hydrographical and dynamical regime in which the campaign took place. Figure 4 shows the SST, chl-a and turbidity. From turbidity we can locate the river plumes of the Adour and the Bidasoa rivers. The LRC derived from the HF radar give a high-resolution image of the surface movement for the previous 3 days, encompassing two periods, July 26-29^{th} and July 31^{th} to August 2^{nd}. The LRC provide an essential insight about the time-evolving surface circulation and position of the river plume. The campaign took place during a transitional stage, during the first period (Figure 4 – left column) with north-westerly winds the circulation is somewhat chaotic. This circulation regime shows two cyclonic eddies, located in our sampling area (C17W at 43.7^{o}N and 2^{o}W and C17E at 1.7^{o}W). During the second period (Figure 4 – right column), the shift to north-easterly winds generate a drastic transition to westward currents. At this moment, the eddies are not visible by the HF radar. And instead, in their position we observe a meandering pattern that affects the distribution of the SST; as well as, the position of the river plumes and its associated chl-a distribution. In addition, on August 2^{nd} a sharp change in SST is observable close to the French inner shelf, which is linked with the upwelling generated by the north-easterly winds.

The first meters of the water column were characterized by a high spatial variability (Figure 5). Although the river plume is not visible anymore in the salinity fields at 14 m, a filament-like layer of relatively fresh water (<35.1 psu) is located in the inner continental shelf (1.6 – 1.7^{o}W). It is surrounded by saltier waters of the open ocean on the east and slightly saltier at the west, leading to a surface salinity front. At 60 m depth (Figure 5 top-right, a second salinity front is observed, this time

https://doi.org/10.5194/os-2020-58
Preprint. Discussion started: 18 June 2020

coinciding with the shelf break, located approximately along the - 250 m isobath. The salinity range in the shelf break front is much smaller than in the surface front.

The presence of the cyclones depicted in Figure 4 is also evidenced at deeper layers. While it is not appreciated in the temperature fields, their existence is clearly represented by vorticity and geostrophic velocities. Interestingly, their position is similar to the one observed by the HF radar during the period 26^{th}-29^{th} of July, just before the campaign. The disappearance of the C17W and C17E in the LRC fields during the campaign period coincides with a change in wind the wind pattern and this might be masking the geostrophic circulation at surface. The meandering pattern already described might be resulting from a combination of both the cyclonic circulation and the surface ageostrophic currents generated by the wind. Few days after, once the wind pattern changes again back to a north-west component, C17W is observable again in the HF radar (See Supplementary Material Figure A1), displaying a persistent nature. Noteworthy, the vorticity fields also show an anticyclone (A17) the NW part of the domain (centred at 43.80^{o}N 2.25^{o}W), however this is not observed in the HF radar fields. At greater depth the cyclones are still noticeable, although they become progressively weaker. In addition to the anticyclone A17, a region of anticyclonic vorticity is well defined in the fontal area between the cyclones. At 60 m the cyclonic eddies present a negative temperature anomaly and relative higher salinity values. The eddy A17 is associated to a positive temperature anomaly and higher salinity. Associated to the frontal areas in the two dipoles (A17-C17W and C17W-C17E) we observe main upwelling areas (positive vertical velocities) which maxima have a relatively constant position throughout the water column.

From the cross-section at 43.77^{o}N we can observe the vertical extension of both the low salinity surface front and the shelf break salinity front (Figure 6A). The surface salinity front has a vertical extension of $\sim$20 m while the location of the shelf break front ranges from $\sim$50 to 110 m. The uplift and depression of the isopicnal lines (black contours) is coherent with the presence of mesoscale structures of different polarity, mostly following the temperature distribution. These two variables contribute to the water density and the position of the seasonal pycnocline at $\sim$25 m, primarily conditioned by the warming of surface waters in summer. The pycnocline is slightly uplift in the western side of the domain, while the isopycnals located deeper below are depressed. These are spatially correlated with the position of the salinity maximum and the A17 eddy. From the vorticity field and the geostrophic meridional velocities (Figure 6 lower left and contours), it is noticed that the position of the anticyclonic frontal area between C17W and C17E coincides with the shelf break (1.9^{o}W) and its strength decreases with depth from a maximum at 25 m. The onshore area is dominated by a southward flow while in the offshore area northward flow is predominant. As in Figure 5, the highest vertical velocities are located in the periphery of the eddies, there where the largest vorticity gradients are located. Both magnitude (O(1-10) m/d) and location of the calculated vertical velocities are consistent with already reported results (Mahadevan et al., 2008; Lévy et al., 2012; Caballero et al., 2016).

3.2 Observed phytoplankton distribution

During the campaign the phytoplankton distribution the SE-BoB is heterogeneous both spatially and temporally. Rivers provide dissolved river-borne nutrients that boost primary production. At the same time, coastal chl-a is highly dependent on the

https://doi.org/10.5194/os-2020-58
Preprint. Discussion started: 18 June 2020

seasonality of river discharge (Guillaud et al., 2008). The fluorescence and salinity data collected at surface by the continuous recording system provides a synoptic distribution of the phytoplankton during the sampling period (2 - 4th of August 2017). Figure 7 illustrates how the phytoplankton distribution is spatially dependent on the position of the river plume at 3.5 m depth. The maximum fluorescence is observed around the salinity minimum, decreasing to the NW (and with the depth) in accordance with the increase of salinity.

Performing a cross-section at the same location as for the hydrographic and hydrodynamic data, provides an image of the spatial distribution of the phytoplankton community (Figure 8). The distribution is complex, two Deep Chlorophyll Maximum (DCM) are observed, one at the inner shelf at 30-50 m, and the second located at the shelf edge at 50-65 m, below the pycnocline. At the same time, the shallow DCM seems to be split into two cores, although its morphology is hard to asses due to the limited spatial coverage of the sampling. However, this patchy distribution correlates at some extent with the areas of minimum vorticity, where the deepest DCM at the shelf break is located at anticyclonic frontal area between C17W and C17E. Regarding the composition of the DCMs, a major fraction of the total fluorescence is resulting from the brown algae, the dominant group. The maximum is again centred in the anticyclonic frontal area, particularly between C17W and C17E. Green algae, however, follow a different pattern and is distributed slightly deeper, following the salinity contours at waters saltier than 35.49. The ratio between brown algae and green algae (B:G), logarithmically normalized, provides an even clearer image of how the different phytoplankton communities are distributed. There is a sharp transition between the brown algae dominated area around the anticycloninc frontal area and the green algae dominated area below the 35.55 halocline. A cross section at the 43.70 ^{o}N (See Suplementary Material Figure A2), out of the core of the anticyclonic frontal area, revels that this pattern is not ubiquous. Here there is not a clear dichotomy among the groups nor a deeper maximum of green algae.

3.3 Exploring bio-physical interactions

From satellite imagery and continuously recorded surface salinity and fluorescence data (Figure 4 and 8), we identify salinity as the main modulating factor for phytoplankton distribution in the surface-most layer. However, the deeper we go the more factors come to interplay and the less importance salinity has modulating phytoplankton distribution. The presence of a seasonal pycnocline determines the mixed layer depth and the occurrence of two dynamically different sections that need to be analysed separately in order to constrain the different dynamical environments. Above the pycnocline the geostrophic processes have a reduced relevancy as can be covered by non-geostrophic processes related to wind-driven currents (e.g. offshore advection of coastal waters during upwelling-favourable winds) which show decreasing intensity with depth. Thus, below pycnocline, we could expect geostrophic currents progressively become the main driver for particle advection. These two sections are also different regarding the nutrient supply. Typically, waters above the mixed layer are depleted in nutrients, whereas below, the phytoplankton would benefit from the nutrient supply by ocean deep waters in combination with maximum light penetration in summer(Cullen, 2015). This can also lead to different phytoplankton communities with different nutrient requirements.

https://doi.org/10.5194/os-2020-58
Preprint. Discussion started: 18 June 2020

The different environments among the water column motivated us to divide the dataset between the two different dynamics areas of the section "Above the pycnocline" and "Below the pycnocline". These two sections were modelled separately through the GAMs.

3.3.1 Bio-physical interaction at the surface layer

The GAMs shown in Figure 9 correspond to the section "Above the Pycnocline" where low salinity values exert a potentially greater impact in fluorescence and in phytoplankton accumulation and growth. As the salinity increases, the fluorescence-estimated chlorophyll concentration decreases, as a result high fluorescence values are observed in the area of influence of the river run-off close to the surface. Brown algae present the highest concentrations around the halocline of $\sim$35.1 psu, while green algae follow a similar curve as the total fluorescence, but it flattens where brown algae are more dominant. The positive relation at the edges of the temperature range may correspond to two different communities. One at the most surface layers where water is warmer and phytoplankton concentration is higher. And a second that is favoured by the colder and nutrient rich water, describing the positive effect at low temperatures. Green algae again follow a similar pattern as total fluorescence. Brown algae, however, do not present so high concentrations at surface warm and saltier water. Besides, our vorticity estimates seem to slightly impact the occurrence of phytoplankton as well, the more cyclonic is a water parcel the highest its fluorescence.

Noteworthy, for the two major phytoplankton pigmentary groups, brown and green algae, only salinity and very extreme temperatures exerts a differential response and shapes their distribution. The core of temperature values (20 - 23^{o}C) have very little effect on the distribution of phytoplankton. The B:G ratio clearly represents the distinctive response of these two pigmentary groups, the higher the salinity, the more favour (disfavoured) are the green (brown) algae. However, the relation of the B:G ratio is non-significant. It is also worth remarking that vertical velocities were calculated as well, nonetheless, due to the necessary boundary condition at surface for the calculation, its relations with fluorescence were not realistic and therefore not included in Figure 9.

3.3.2 Bio-physical interaction below the pycnocline

The GAM covering the section below the pycnocline shows rather different behaviour (Figure 10), the positive impact of salinity on phytoplankton is only limited to the lower values in the salinity range (35.4 – 35.6 psu). Although this is the case for the total fluorescence and the brown algae, increasing values of salinity have a positive linear effect on green algae. Noteworthy, the dominant group in these layers is the composed by brown algae and, therefore, its responses almost mimic the ones of the total fluorescence. The response of phytoplankton to temperature is strong, but highly dependent on the location of the DCM in the water column and does not represent a causative relation. Unlike above the pycnocline, here vorticity yields an opposite response for brown and green algae; the more cyclonic is a water parcel, the more beneficial it is for green algae, while an anticyclonic regime would favour the occurrence of brown algae. Against expectations, the vertical velocities do not have a clear impact and the response is rather flat. This is counter-intuitive, since positive vertical velocities -i.e. upwelling- are

https://doi.org/10.5194/os-2020-58
Preprint. Discussion started: 18 June 2020

responsible of bringing nutrients to the euphotic zone, and negative velocities -i.e downwelling- might drive the phytoplankton to deeper leves. Rather, it seems that the distribution and phytoplankton community composition depend on the interplay of salinity and vorticity, as suggested by the relation of the B:G ratio where salinity and vorticity have the major effects.

4 Discussion

The hydrographic and hydrodynamic regime of the South-Eastern corner of BoB during the ETOILE campaign, despite being spatio-temporally highly variable, were not exceptional and similar conditions have been already recorded. The surface salinity front we encountered onshore has been observed and reported before by Reverdin et al. (2013) on early May 2009. They described a fresher (34-35 psu) and deeper (∼30 m) freshwater layer, which signal weaken towards August by increasing salinity to ∼35 psu as a result of vertical mixing and offshore advection by Ekman transport. This surface front is observable on the cross section shown in Figure 6. We consider the low salinity water filament boundary at 35.1 psu, in coherence with the limit used in Puillat et al. (2006) to describe low water lenses in the area. Given this boundary value, we describe a vertical extension of 18 m (34.98 - 35.1 psu), and a horizontal extension over 20 km. In addition to the surface front generated by the river runoff, a second saline front was observed at subsurface (50-120 m), located over the shelf break. Here the fresher water (<35.5 psu) occupy the totality of the water on the shelf, in comparison with the oceanic water at the slope (>35.6 psu). This shelf break front seems to correspond to a persistent feature in the study area due to the differences between the waters over the French shelf and Landes Plateau and those located over the Spanish shelf and slope (Valencia et al., 2004).

Furthermore, the dipole-type structures have also been observed before in the BoB, yet in a larger scale (Caballero et al., 2016; Pingree and Garcia-Soto, 2014; Solabarrieta et al., 2014; Rubio et al., 2018). While the cyclones are detected by the HF radar before the campaign, these vanish when the circulation changes due to the change in wind regime. Their intermittent signature in the HF radar surface fields is explained by the interaction of the geostrophic and wind induced flow. A similar situation was described using an analytical model in the Florida current by Yonggang et al. (2015), showing a surface meandering flow as a result of the overlap between a coastal jet and a eddy dipole field. This is coherent with our observations, where, with predominant NE winds the wind-driven circulation over the eddy field results in a meandering structure. Indeed, as the wind weakens the cyclones signature is again observed in the HF radar fields .

The observed field during the ETOILE campaign could be resultant of the dominance of non-linear terms in frontal system (Lévy et al., 2001), response from the interaction of the IPC and the abrupt bathymetry (Rubio et al., 2018). Moreover, the structure A17 has the characteristics of the SWODDIES, i-.e., an uplift of the seasonal pycnocline while deeper isopycnals are depressed and a salinity maximum in the core. Nevertheless, it is not straightforward to discern the triggering processes behind the generation of the observed structures. The closeness to the shore and the frontal system itself might alter the eddy circu-

https://doi.org/10.5194/os-2020-58
Preprint. Discussion started: 18 June 2020

lation and results in a complex eddy field to interpret. In addition, the sampling is limited both in temporal and spatial coverage.

The described hydrographic and dynamic conditions affect significantly the phytoplankton distribution, although the interplay between phytoplankton and physics seems to vary significantly depending on the location in the water column. The surface layer in the SE corner of BoB is a Region of Fresh Water Influence (ROFI), mainly modulated by the presence of a riverine freshwater source in the area that highly shapes phytoplankton distribution through river-borne nutrient supply. Ultimately, the location of the Adour and Bidasoa river plumes is dependant of the wind conditions, which controls the non-geostrophic surface circulation as shown by the LRC. Our results agree with the observed general pattern in which westerly winds push the turbidity plume towards the coast (Figure 8 left column), while northerly winds promote an offshore expansion (Figure 8 right column) (Petus et al. (2014)). Salinity is the main modulating factor from the surface-most layer of the ROFI to the pycnocline. The impact of the ROFI is extended via the presence of the low salinity filament. The effect of salinity on phytoplankton distribution is maintained as we go deeper in the water column, although the GAM analysis also shows a dependence with the vorticity. While relatively weak, the response of the brown algae to vorticity above the pycnocline is opposite to the one observed below – i.e higher abundance at more cyclonic location. We believe this relation reflects the potential of eddies to modify the low salinity -and nutrient rich- filament position at surface.

Given that the conditions at the DCM would be in theory optimal for phytoplankton growth, we followed an approach that let us decouple the relative effect that salinity and vorticity have in modulating phytoplankton community. This is done from a synoptic perspective, without trying to explain the triggering factor given the interdependence of salinity and vorticity. We decreased the size of the dataset located below the pycnocline by omitting the points in which the total fluorescence value is lower than a certain filter value. The filter value ranges from the fluorescence minimum to its maximum, and it increases subsequently at each iteration. Thereby, we filter out points with low fluorescence values, reducing the dataset in size while maintaining its 3-D complexity. At the same time, each iteration the dataset is more and more confined to DCM values. At each selected filter value, we carried out a Pearson's linear correlation between green and brown algae (Figure 11 - left) and the B:G ratio (Figure 11 - right) and the affecting factors salinity and vorticity. Note that only correlation coefficients with significant values (p-value$<$0.05) are present in Figure 11.

At very small iteration numbers most of the data is conserved, generally small and uncorrelated values add "noise" and decrease the value of coefficient. With this approach we were able to filter out this noise and understand the factors underlying in the DCM. Although in general, when a small or no filter has been applied the correlations are weak, this is not the case for brown algae. The strong negative correlation points suggest that in general brown algae are highly conditioned by the salinity range. This relation was also observed in the GAM for below the pycnocline, where the magnitude of the effect of salinity was higher in brown than green algae. The relation between the B:G ratio with either of the analysed factor at small filter values is inexistent. Once all the points below 0.7 have been filtered out, the correlations of the B:G ratio towards salinity and vorticity increases, resulting from the differential responses of brown and green algae. While the correlations for green algae increase

https://doi.org/10.5194/os-2020-58
Preprint. Discussion started: 18 June 2020

at similar pace, the salinity is less and less correlated with brown algae. When the value of the filter is set at 1.5, the dataset is only representative of the DCM. Here, there is the minima in the correlation between vorticity and salinity and brown algae. A negative correlation imply that the more negative the vorticity values (or the more anticyclonic) the highest the fluorescence (or the phytoplankton abundance). In opposition, the correlation coefficient between brown algae and salinity shifts towards more neutral values. Although this is also shown in the GAM, this approach describes how vorticity is the major modulating factor for the brown algae under the pycnocline. At this point there is also a change in the correlation of the B:G ratio, at 1.5 the vorticity is more strongly correlated than what salinity is. Therefore around 20% of the data (Figure 11 – right), corresponding to the DCM, is mainly condition by a dynamical factor such as vorticity.

Vorticity stands out as a main conditioning factor of the observed fluorescence distributions, whereas vertical velocities show no direct effect. This could be counter-intuitive at first, frontal regions are characterized by the presence of sub-mesoscale processes that could have a key role in modulating mixing conditions and nutrient provision and thus creating a favourable environment for phytoplankton growth. Our observations show that vertical velocities are maximum at the cyclonic eddy's peripheries, in agreement with several studies, which relate this vertical velocities to (sub)mesoscale physical processes (Lévy et al., 2001; Mahadevan et al., 2008; Caballero et al., 2016). However, the highest phytoplankton concentration does not coincide with the areas of vertical velocities. Even if upwelling does bring nutrient rich waters to the euphotic zone, the phytoplankton concentration that these waters carry could be very low. And in order to grow and multiply, algae need time during which the water parcel might be transported away from the upwelling area (Omta et al., 2008). This would explain the lack of correlation between the vertical velocities and the phytoplankton occurrence is observed during ETOILE. Therefore we argue that there must be a third process that mediates between the provisioning of nutrients by the vertical velocities and the phytoplankton distribution. This process should also explain the relation of vorticity and fluorescence.

Different physical processes can provide the link between vorticity and phytoplankton occurrence in the centre of anticyclonic structures. McGillicuddy et al. (2007) attributed the existence of a DCM in the centre of the anticyclones to eddy/wind interactions; whereby, the wind stress varies on diametrically opposite sides of the anticyclone driving a vertical nutrient flux through Ekman Pumping. This has been more recently observed by Caballero et al. (2016), associated to a larger scale SWODDIEs in the BoB during winter. Although the anticyclone A17 at 2.25^{o}W presents the characteristics of a SWODDIE like eddy, no fluorescence measurements were collected as far as this longitude. In addition, due to the strong summer pycnocline observed in our case, it is considered that the effect of wind at depths of the DCM was negligible, and thus another process must trigger the phytoplankton maximum.

Besides, various models have obtained similar results to the ones we observed. Using a numerical model Mahadevan et al. (2008) reported that although upwelling and new production are more pronounced in the periphery of the eddies (frontal areas), phytoplankton gathers up in the centre of anticyclones, showing a clear decoupling between upwelling and the associated primary production and phytoplankton accumulation. Even if the largest vertical velocities occur at the periphery, a small radially

https://doi.org/10.5194/os-2020-58
Preprint. Discussion started: 18 June 2020

inward component of velocity causes plankton to be transported towards the eddy centre. Our vorticity observations agree with the proposed bio-physical interaction, the anticyclone frontal area observed between the two cyclones may provoke the advective accumulation of phytoplankton in its centre. And in addition, it could also provide a fluid dynamical niche with the right conditions of nutrient and turbulence where brown algae can flourish and outcompete the green algae. Therefore, the largest concentrations of plankton can build up in the eddy centre even with nutrient supply at the periphery (Mahadevan et al., 2008; Lévy et al., 2012).

It is also important to remind that the formation and maintenance of the DCM is not only depend on nutrient availability but also rely strongly on photo-acclimation of pigment content that could lead to elevated chlorophyll concentration relative to phytoplankton biomass at depth (Cullen, 2015), which could, together with variable fluorescence to chlorophyll ratios (**?**), amplify the accumulation signal recorded. All these features, including different swimming behaviour and/or buoyancy control, can lead to specific aggregations of phytoplankton in layers which, in turn, are subject to differential grazing and physical control (Cullen, 2015; Latasa et al., 2016). Most likely, our results encompass an interplay of different bio-physical interactions. According to Latasa et al. (2017), diatoms ocurring in canyons areas should be well adapted to thrive the pulsing and dynamical environment and could manage to stay above their theoretical depth if just constant nutrient diffusion takes place. During our cruise, brown algae, which often showed show indeed a maximum depth shallower than green algae, were mostly represented by diatoms but also by dinoflagellates (Gómez, unpubl. Data). The latter can easily regulate their optimum depth by altering their swimming behaviour. Concerning the green algae group, Cabello et al. (2016) in a similar system, found that chlorophytes were able to show a broad vertical distribution with a not very pronounced peak at the DCM and sometimes two maximas separated by several meters within this layer, suggesting the presence of different segregated populations of chlorophytes in the DCM layer. Moreover, they remind that pelagophytes are known to be able to use the low-light high-nutrient conditions typical of this layer. These studies confirm that different phytoplankton groups of different ecological needs and traits are well adapted to the potential different microenvironments characterising this DCM layer of strong abiotic gradients (Latasa et al., 2017).

It is worth remarking the main limitations encountering during this study, especially focusing in the ETOILE campaign. The area covered by the sampling was insufficient for completely resolve some of the observed structures. Similarly, having just a synoptic image of the processes and lacking temporal information (despite operational and remote sensing data) makes challenging to derive a cause-consequence relation, especially regarding the evolution of the system. Although we could quantify, to a certain extent, different phytoplankton pigmentary groups, no further classification was carried out as no phytoplankton counts nor pigment analysis were effective at different depths, which might have help correlating spectrally-defined groups to real pigmentary groups and/or taxa. This is an essential issue to be considered, since Fluoroprobe factory fingerprints are determined on mono-specifical cultures or target micro-algae which are not necessarily representative to our shelf and ocean system. In addition, these fingerprints show a relatively important variability amongst species of a single spectral group and even amongst population of the same species (**?**). No nutrient or light measurements where taken either, and therefore we

https://doi.org/10.5194/os-2020-58
Preprint. Discussion started: 18 June 2020

cannot explicitly describe any inter-species competition which will help us understanding the ecological consequences of these (sub)mesoscale processes. In any case, vorticity creates a dynamical niche that plays a major role shaping the phytoplankton community. A distinct community structure was anyway detected, compared to the surrounding water, which could potentially be extent through the trophic web and even affect top predator's foraging behaviour (Cotté et al., 2015; Tew Kai et al., 2009). Thus, the combined effects of (sub)mesoscale features, even though a relatively small fraction of the total area, may be disproportionately important to biological dynamics.

Understanding the dynamical fluid niches is essential for the correct comprehension of the ecosystem. Certain algae may find their niches not only in surface, as pointed out by D'Ovidio et al. (2010) but also at the ocean interior. Assessing group specific bio-physical interactions are also of high relevance for developing and constraining the "Plankton Functional Types" (PFTs) used in ocean biogeochemistry and climate prediction models (Le Quere et al., 2005). In addition, if among these algae we include the species causing Harmful Algae Blooms, the correct evaluation and monitoring of these structures as well as their effects in different phytoplankton species becomes critical for the ecosystem and human health.Previous studies have report similar hydrographic conditions in the same area, suggesting that the processes we have identify might be at least seasonally recurrent (Fernández et al., 1993; Valencia et al., 2004). Consequently, and given the economic importance of the fisheries sector in the adjacent coastal areas of Spain and France, we address the need of a more exhaustive study in the area, highlighting the importance of crossing plankton and dynamic data.

5 Conclusions

In the present study we conducted a joint analysis of remote and operational together with discrete data to reconstruct the mesoscale and submesoscale processes and the influence exerted on the phytoplankton community (followed at high spatial resolution by multi-spectral fluorometry) in the South-Eastern Bay of Biscay. Satellite imagery provides information about the surface-most layer, which is highly conditioned by the run-off of Adour and Bidasoa rivers. The location of the plume depends on the surface currents, which are ultimately conditioned by the direction of the wind. In addition, wind can also affect the phytoplankton distribution by the creation of low salinity lenses via coastal upwelling and their subsequent offshore transport.

From top to bottom salinity plays a major role shaping the phytoplankton community. It acts as a conditioning factor in the community, having contrasting effects for the different phytoplankton groups that compose it. While above the pycnocline, the only affecting the community composition is salinity, below the pycnocline the geostrophic processes gain relevance. Vorticity is the most correlated factor affecting not only the spatial location of the Deep Chlorophyll Maxima, since it is associated with the anticyclonic circulation, but also affecting the spectral composition of the community. This research brings into consideration the relevance of the dynamic variables in the study of phytoplankton, decoupling the processes at surface and subsurface, as well as the interest of observing phytoplankton at high spatial resolution. We also address the importance of in situ data of

https://doi.org/10.5194/os-2020-58
Preprint. Discussion started: 18 June 2020

these characteristics in order to construct the complete 3D picture of the distribution and composition of the phytoplankton community. Further investigations on the fine structure of the DCM will help to better identify the ecological and functional traits of phytoplankton groups. It is clear that the vertical alignment of phytoplankton groups preclude considering the DCM as a homogeneous layer.

Appendix A: Supplementary Material

A1 Observation of eddies after ETOILE

After the change in wind regime on August 7^{th} the eddy C17W is again visible in the HF radar. Its has moved southwards with respect its location on July 29^{th}. Meanwhile, C17E has vanished although it might be just masked by the surface currents since a meandering is still visible in its former location at 1.7^{o}W.

A2 Phytoplakton Observations at T3

A cross section at the 43.70 ^{o}N (See Suplementary Material Figure A2), out of the core of the anticyclonic frontal area, revels that this pattern is not ubiquous. Here there is not a clear dichotomy among the groups nor a deeper maximum of green algae. Rather, there is a uniform layer of brown algae.

Author contributions. XD, AR, FA, IP, IMN, PL and AC contributed to the main structure and contents. In addition, XD produced the figures and IP and PL coordinated the cruise.

Competing interests. The authors declare that they have no conflict of interest.

Acknowledgements. This project was supported by the JERICO-NEXT (Joint European Research Infrastructure for Coastal Observatory – Novel European eXpertise for coastal observaTories) project within the European Union's Horizon 2020 research and innovation programme (grant agreement no. 654410). SST and Chl-a data are produced and distributed by NERC Earth Observation Data Acquisition and Analysis Service (NEODAAS, https://www.neodaas.ac.uk/Access_Data). We thank the Emergencies and Meteorology Directorate – Security department – Basque Government for public data provision from the Basque Operational Oceanography System EuskOOS. Ivan Manso-Narvarte was supported by a PhD fellowship from the Department of Environment, Regional Planning, Agriculture and Fisheries of the Basque Government. We would like to thank everyone who participated in the ETOILE Campaign and has collected or processed the data as well as the

https://doi.org/10.5194/os-2020-58
Preprint. Discussion started: 18 June 2020

“cote de la Manche” crew. This is the contribution number XXX of the Marine Research Division of AZTI-Tecnalia.

https://doi.org/10.5194/os-2020-58
Preprint. Discussion started: 18 June 2020

References

Benson, D. J.: Computational methods in Lagrangian and Eulerian hydrocodes, Computer Methods in Applied Mechanics and Engineering, 99, 235–394, https://doi.org/10.1016/0045-7825(92)90042-I, 1992.

Caballero, A., Ferrer, L., Rubio, A., Charria, G., Taylor, B. H., and Grima, N.: Monitoring of a quasi-stationary eddy in the Bay of Biscay by means of satellite, in situ and model results, Deep-Sea Research Part II: Topical Studies in Oceanography, 106, 23–37, https://doi.org/10.1016/j.dsr2.2013.09.029, 2014.

Caballero, A., Rubio, A., Ruiz, S., Le, B., Testor, P., Mader, J., and Hernández, C.: South-Eastern Bay of Biscay eddy-induced anomalies and their effect on chlorophyll distribution, Journal of Marine Systems, pp. 1–16, https://doi.org/10.1016/j.jmarsys.2016.04.001, 2016.

Cabello, A. M., Latasa, M., Forn, I., Morán, X. A. G., and Massana, R.: Vertical distribution of major photosynthetic picoeukaryotic groups in stratified marine waters, Environmental Microbiology, 18, 1578–1590, https://doi.org/10.1111/1462-2920.13285, 2016.

Cotté, C., D'Ovidio, F., Dragon, A. C., Guinet, C., and Lévy, M.: Flexible preference of southern elephant seals for distinct mesoscale features within the Antarctic Circumpolar Current, Progress in Oceanography, 131, 46–58, https://doi.org/10.1016/j.pocean.2014.11.011, 2015.

Cullen, J. J.: Subsurface Chlorophyll Maximum Layers: Enduring Enigma or Mystery Solved?, Annual Review of Marine Science, 7, 207–239, https://doi.org/10.1146/annurev-marine-010213-135111, 2015.

D'Ovidio, F., De Monte, S., Alvain, S., Dandonneau, Y., and Levy, M.: Fluid dynamical niches of phytoplankton types, Proceedings of the National Academy of Sciences, 107, 18 366–18 370, https://doi.org/10.1073/pnas.1004620107, 2010.

Emery, W. J. and Thomson, R. E.: Preface, in: Data Analysis Methods in Physical Oceanography, edited by Emery, W. J. and Thomson, R. E., Elsevier Science, Amsterdam, https://doi.org/https://doi.org/10.1016/B978-044450756-3/50000-9, 2001.

Fernández, E., Cabal, J., Acuña, J. L., Bode, A., Botas, A., and García-soto, C.: Plankton distribution across a slope current-induced front in the southern Bay of Biscay, Journal of Plankton Research, 15, 619–641, https://doi.org/10.1093/plankt/15.6.619, 1993.

Ferrer, L. and Caballero, A.: Eddies in the Bay of Biscay: A numerical approximation, Journal of Marine Systems, 87, 133–144, https://doi.org/10.1016/j.jmarsys.2011.03.008, 2011.

Garcia-Soto, C.: Navidad development in the southern Bay of Biscay: Climate change and swoddy structure from remote sensing and in situ measurements, Journal of Geophysical Research, 107, 3118, https://doi.org/10.1029/2001JC001012, 2002.

Gomis, D. and Ruiz, S.: Manual DAToBJETIVO v.01: Una herramienta para el análisis espacial objetivo y diagnóstico de variables oceanográficas. Departamento Recursos Naturales, Grupo de Oceanografía Interdisciplinar IMEDEA (centro mixto Universitat de les Illes Balears - CSIC), Mallorca, España., 2003.

Gomis, D., Ruiz, S., and Pedder, M. A.: Diagnostic analysis of the 3D ageostrophic circulation from a multivariate spatial interpolation of CTD and ADCP data, Deep-Sea Research Part I: Oceanographic Research Papers, 48, 269–295, https://doi.org/10.1016/S0967-0637(00)00060-1, 2001.

Guillaud, J.-f., Aminot, A., Delmas, D., Gohin, F., Lunven, M., Labry, C., and Herbland, A.: Seasonal variation of riverine nutrient inputs in the northern Bay of Biscay (France), and patterns of marine phytoplankton response, 72, 309–319, https://doi.org/10.1016/j.jmarsys.2007.03.010, 2008.

Hastie, T. and Tibshirani, R.: Generalized Additive Models, Chapman and Hall, 1990.

https://doi.org/10.5194/os-2020-58
Preprint. Discussion started: 18 June 2020

Irigoien, X., Fiksen, Cotano, U., Uriarte, A., Alvarez, P., Arrizabalaga, H., Boyra, G., Santos, M., Sagarminaga, Y., Otheguy, P., Etxebeste, E., Zarauz, L., Artetxe, I., and Motos, L.: Could Biscay Bay Anchovy recruit through a spatial loophole?, Progress in Oceanography, 74, 132–148, https://doi.org/10.1016/j.pocean.2007.04.011, 2007.

Latasa, M., Gutierrez-Rodriguez, A., Cabello, A. M., , and R, S.: Influence of light and nutrients on the vertical distribution of marine phytoplankton groups in the deep chlorophyll maximum, Sci. Mar. 80S1, pp. 57–62, https://doi.org/10.3989/scimar.04316.01A, 2016.

Latasa, M., Cabello, A. M., Morán, X. A. G., Massana, R., and R, S.: Distribution of phytoplankton groups within the deep chlorophyll maximum, Limnology and Oceanography, pp. 665–685, https://doi.org/10.1002/lno.10452, 2017.

Le Quere, C., Harrison, S., Prentice, I. C., Buitenhuis, E. T., Aumont, O., Bopp, L., Claustre, H., Cotrim Da Cunha, L., Geider, R., Giraud, X amd Klaas, C., Kohfeld, K. E., Legendre, L., Manizza, M., Platt, T., B, R. R., Sathyendrannath, S., Uitz, J., Watson, A. J., and Wolf-Gladrow, D.: Ecosystem dynamics based on plankton functional types for global ocean biogeochemistry models, Global Change Biology, 11, 2016–2040, https://doi.org/10.1111/j.1365-2486.2005.01004.x, 2005.

Lévy, M., Klein, P., and Treguier, A.-M.: Impact of sub-mesoscale physics on production and subduction of phytoplankton in an oligotrophic regime, Journal of Marine Research, 59, 535–565, https://doi.org/10.1357/002224001762842181, 2001.

Lévy, M., Ferrari, R., Franks, P. J., Martin, A. P., and Rivière, P.: Bringing physics to life at the submesoscale, Geophysical Research Letters, 39, 1–13, https://doi.org/10.1029/2012GL052756, 2012.

Llope, M., Chan, K., and Reid, P. C.: Effects of environmental conditions on the seasonal distribution of phytoplankton biomass in the North Sea, 54, 512–524, 2009.

Llope, M., Licandro, P., Chan, K. S., and Stenseth, N. C.: Spatial variability of the plankton trophic interaction in the North Sea: A new feature after the early 1970s, Global Change Biology, 18, 106–117, https://doi.org/10.1111/j.1365-2486.2011.02492.x, 2012.

Mahadevan, A.: Ocean science: Eddy effects on biogeochemistry, Nature, 506, 168–169, https://doi.org/10.1038/nature13048, 2014.

Mahadevan, A.: The Impact of Submesoscale Physics on Primary Productivity of Plankton, Annual Review of Marine Science, 8, https://doi.org/10.1146/annurev-marine-010814-015912, 2016.

Mahadevan, A., Thomas, L. N., and Tandon, A.: Comment on "eddy/wind interactions stimulate extraordinary mid-ocean plankton blooms", Science, 320, https://doi.org/10.1126/science.1148974, 2008.

McGillicuddy, D. J., Anderson, L. A., Bates, N. R., Bibby, T., Buesseler, K. O., Carlson, C. A., Davis, C. S., Ewart, C., Falkowski, P. G., Goldthwait, S. A., Hansell, D. A., Jenkins, W. J., Johnson, R., Kosnyrev, V. K., Ledwell, J. R., Li, Q. P., Siegel, D. A., and Steinberg, D. K.: Eddy/Wind Interactions Stimulate Extraordinary Mid-Ocean Plankton Blooms, Science, 316, 1021–1026, https://doi.org/10.1126/science.1136256, 2007.

Morozov, E., Pozdnyakov, D., Smyth, T., Sychev, V., and Grassl, H.: Space-borne study of seasonal, multi-year, and decadal phytoplankton dynamics in the Bay of Biscay, International Journal of Remote Sensing, 34, 1297–1331, https://doi.org/10.1080/01431161.2012.718462, 2013.

Muller, H., Blanke, B., Dumas, F., Lekien, F., and Mariette, V.: Estimating Lagrangian Residual Circulation (LRC) in the Iroise Sea, Proceedings of the IEEE Working Conference on Current Measurement Technology, 78, 279–284, https://doi.org/10.1109/CCM.2008.4480881, 2009.

Omta, A. W., Kooijman, S. A. L. M., and Dijkstra, H. A.: Critical turbulence revisited: The impact of submesoscale vertical mixing on plankton patchiness, Journal of Marine Research, 66, 61–85, https://doi.org/10.1357/002224008784815766, 2008.

https://doi.org/10.5194/os-2020-58
Preprint. Discussion started: 18 June 2020

Petus, C., Marieu, V., Novoa, S., Chust, G., Bruneau, N., and Froidefond, J. M.: Monitoring spatio-temporal variability of the Adour River turbid plume (Bay of Biscay, France) with MODIS 250-m imagery, Continental Shelf Research, 74, 35–49, https://doi.org/10.1016/j.csr.2013.11.011, 2014.

Pingree, R. D. and Garcia-Soto, C.: Plankton blooms, ocean circulation and the European slope current: Response to weather and climate in the Bay of Biscay and W English Channel (NE Atlantic), Deep-Sea Research Part II: Topical Studies in Oceanography, 106, 5–22, https://doi.org/10.1016/j.dsr2.2014.07.008, 2014.

Puillat, I., Lazure, P., Jégou, A.-m., Lampert, L., and Miller, P.: Mesoscale hydrological variability induced by northwesterly wind on the French continental shelf of the Bay of Biscay, pp. 15–26, 2006.

Reverdin, G., Marié, L., Lazure, P., Ovidio, F., Boutin, J., Testor, P., Martin, N., Lourenco, A., Gaillard, F., Lavin, A., Rodriguez, C., Somavilla, R., Mader, J., Rubio, A., Blouch, P., Rolland, J., Bozec, Y., Charria, G., Batifoulier, F., Dumas, F., Louazel, S., and Chanut, J.: Freshwater from the Bay of Biscay shelves in 2009, Journal of Marine Systems, 109-110, S134–S143, https://doi.org/10.1016/j.jmarsys.2011.09.017, 2013.

Rubio, A., Solabarrieta, L., Castanedo, S., Medina, R., and Aranda, J. A.: SE Bay of Biscay from HF radar data, 2013.

Rubio, A., Caballero, A., Or, A., Hernández-carrasco, I., Ferrer, L., González, M., Solabarrieta, L., and Mader, J.: Remote Sensing of Environment Eddy-induced cross-shelf export of high Chl-a coastal waters in the SE Bay of Biscay, 205, 290–304, https://doi.org/10.1016/j.rse.2017.10.037, 2018.

Sharples, J. and Simpson, J. H.: Periodic Frontogenesis in a Region of Freshwater Influence, Estuaries, 16, 74, https://doi.org/10.2307/1352765, 1993.

Solabarrieta, L., Rubio, A., Castanedo, S., Medina, R., Charria, G., and Hernández, C.: Surface water circulation patterns in the southeastern Bay of Biscay : New evidences from HF radar data, Continental Shelf Research, 74, 60–76, https://doi.org/10.1016/j.csr.2013.11.022, 2014.

Tew Kai, E., Rossi, V., Sudre, J., Weimerskirch, H., Lopez, C., Hernandez-Garcia, E., Marsac, F., and Garçon, V.: Top marine predators track Lagrangian coherent structures, Proceedings of the National Academy of Sciences of the United States of America, 106, 8245–8250, https://doi.org/10.1073/pnas.0811034106, 2009.

Valencia, V., Franco, J., Borja, Á., and Fontán, A.: Hydrography of the southeastern Bay of Biscay, Oceanography and marine environment of the Basque Country, pp. 159–194, https://doi.org/10.1016/S0422-9894(04)80045-X, 2004.

Wood, S.: Fast stable restricted maximum likelihood and marginal likelihood estimation of semiparametric generalized linear models, Journal of the Royal Statistical Society, pp. 3–36, 2011.

Yonggang, L., Kerkering, H., and Weisberg, R.: Chapter 11 - Observing Frontal Instabilities of the Florida Current Using High Frequency Radar, in: Coastal Ocean Observing Systems, edited by Liu, Y., Kerkering, H., and Weisberg, R. H., pp. 179–208, Academic Press, Boston, https://doi.org/10.1016/B978-0-12-802022-7.00011-0, 2015.

https://doi.org/10.5194/os-2020-58
Preprint. Discussion started: 18 June 2020

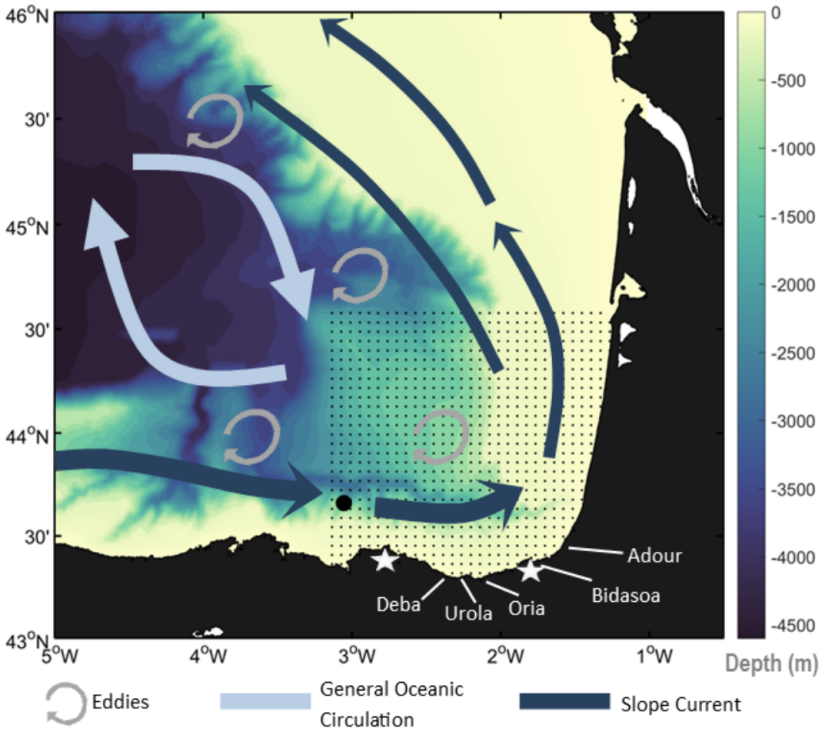

Figure 1. Circulation in the Bay of Biscay. The general circulation is characterized by a weak anticyclonic circulation in the central regions. Costal areas are subjected to a seasonal slope current that, when interacting with the bathymetry results in the generation of eddies.

https://doi.org/10.5194/os-2020-58
Preprint. Discussion started: 18 June 2020

Ocean Science
Discussions
Open Access
EGU

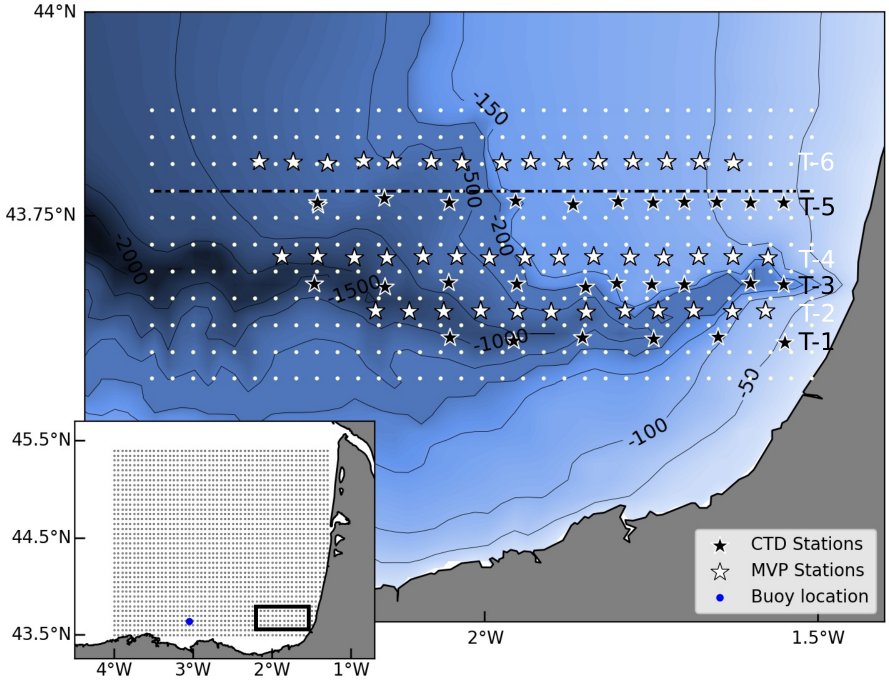

Figure 2. At uneven transects (T-) black stars mark the CTD stations where vertical casts of temperature, salinity and in vivo multi-spectral fluorescence were collected. At even transects, white stars mark the location of the point at which MVP data has been averaged, these are located every 5 km. White dots represent the grid at which these measurements were interpolated and the black dashed line mark the cross-section analysed in the Results Section. The zoomed out map in the lower left corner shows the HF radar grid, where the blue dot is the location of the oceano-metereological buoy used for the wind data and the black square is the study area.

https://doi.org/10.5194/os-2020-58
Preprint. Discussion started: 18 June 2020

Ocean Science
Discussions
Open Access
EGU

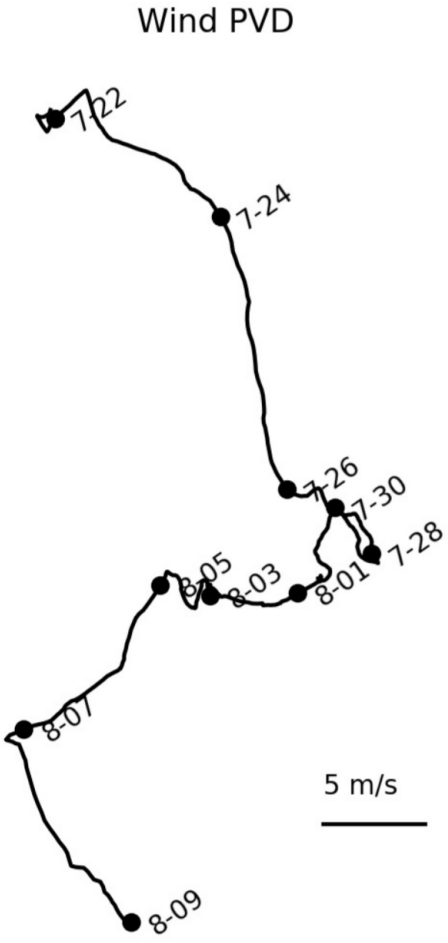

Figure 3. Wind direction and intensity at Bilbao's mooring buoy represented on a Progressive Vector Diagram (PVD).

https://doi.org/10.5194/os-2020-58
Preprint. Discussion started: 18 June 2020

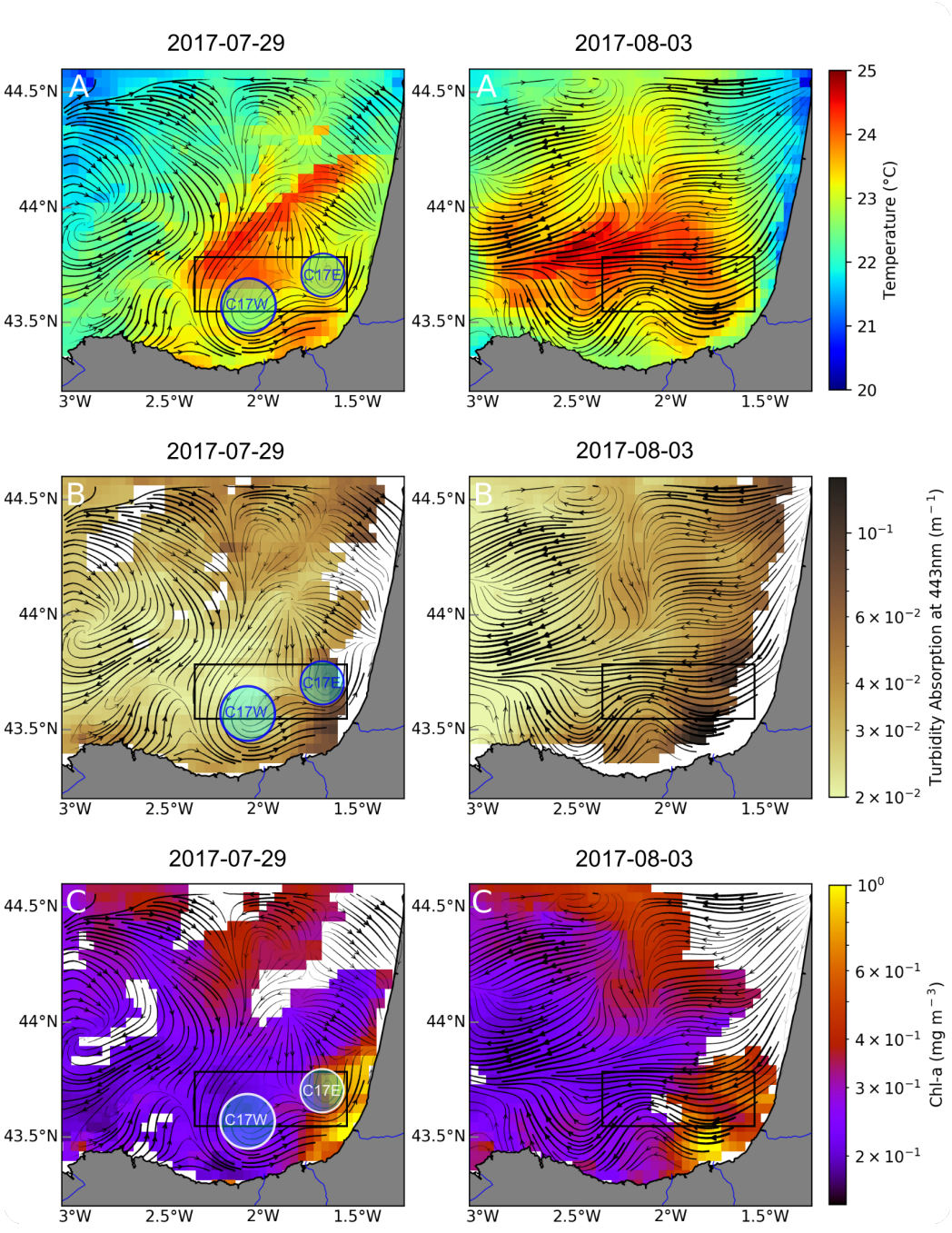

Figure 4. Hydrographic and hydrodynamical context. SST (A), turbidity (B) and Chl-a (C) corresponding to July 29^{th} (left column) and August 2^{nd}. Black lines show the LRC calculated for the previous three days, encompassing to periods; July 26-29^{th} and July 31^{th} to August 2^{nd}. The black box show the study area where the sampling took place.

https://doi.org/10.5194/os-2020-58
Preprint. Discussion started: 18 June 2020

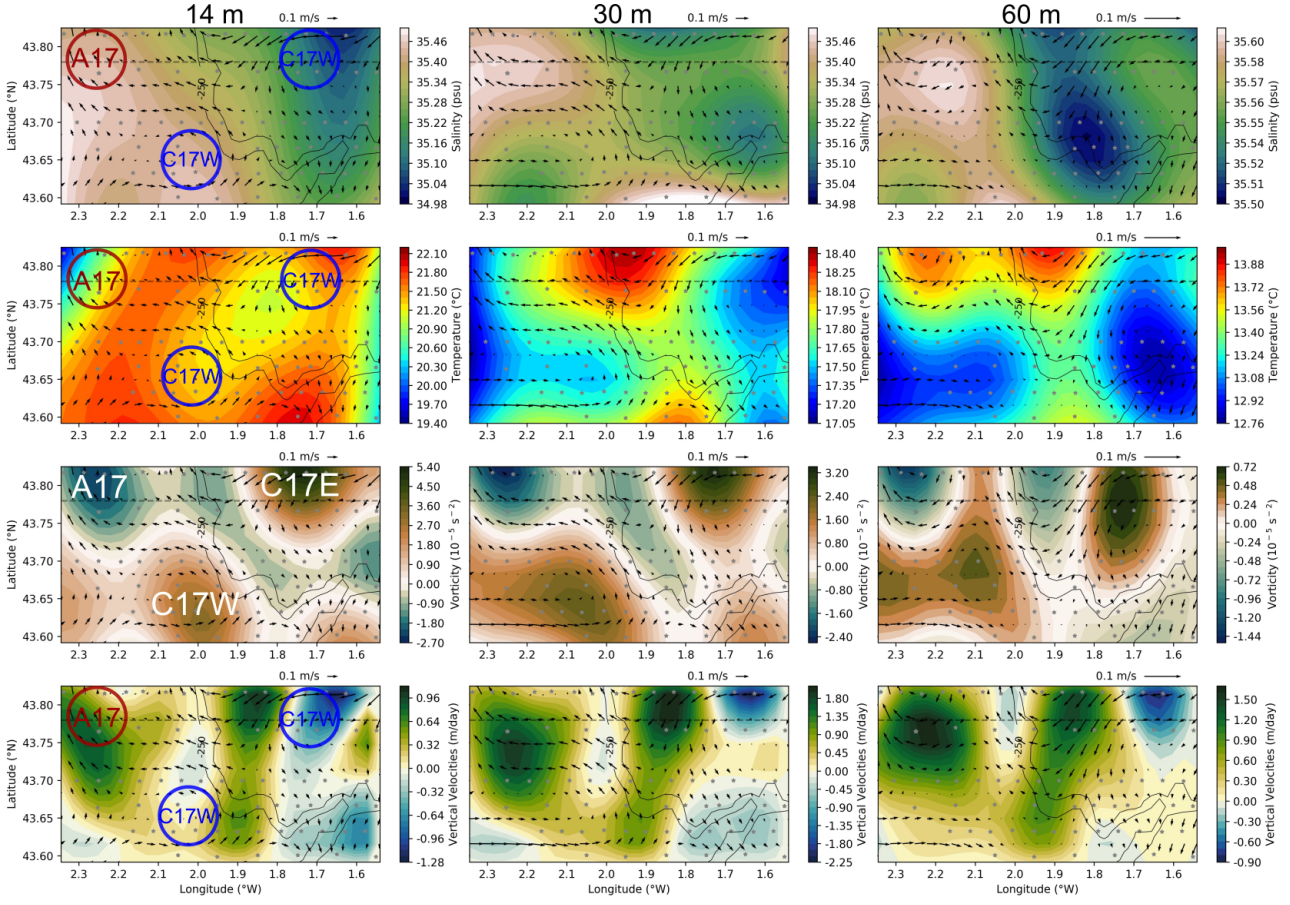

Figure 5. Hydrographic and hydrodynamical context. From top to bottom: salinity, temperature, vorticity and vertical velocity fields. Each of the variables is mapped at 14, 30 and 60 m (left to right). Black arrows correspond to the geostrophic velocities and black contours represent the shelf break. Negative (positive) vorticity values represents anticyclonic (cyclonic) circulation.

https://doi.org/10.5194/os-2020-58
Preprint. Discussion started: 18 June 2020

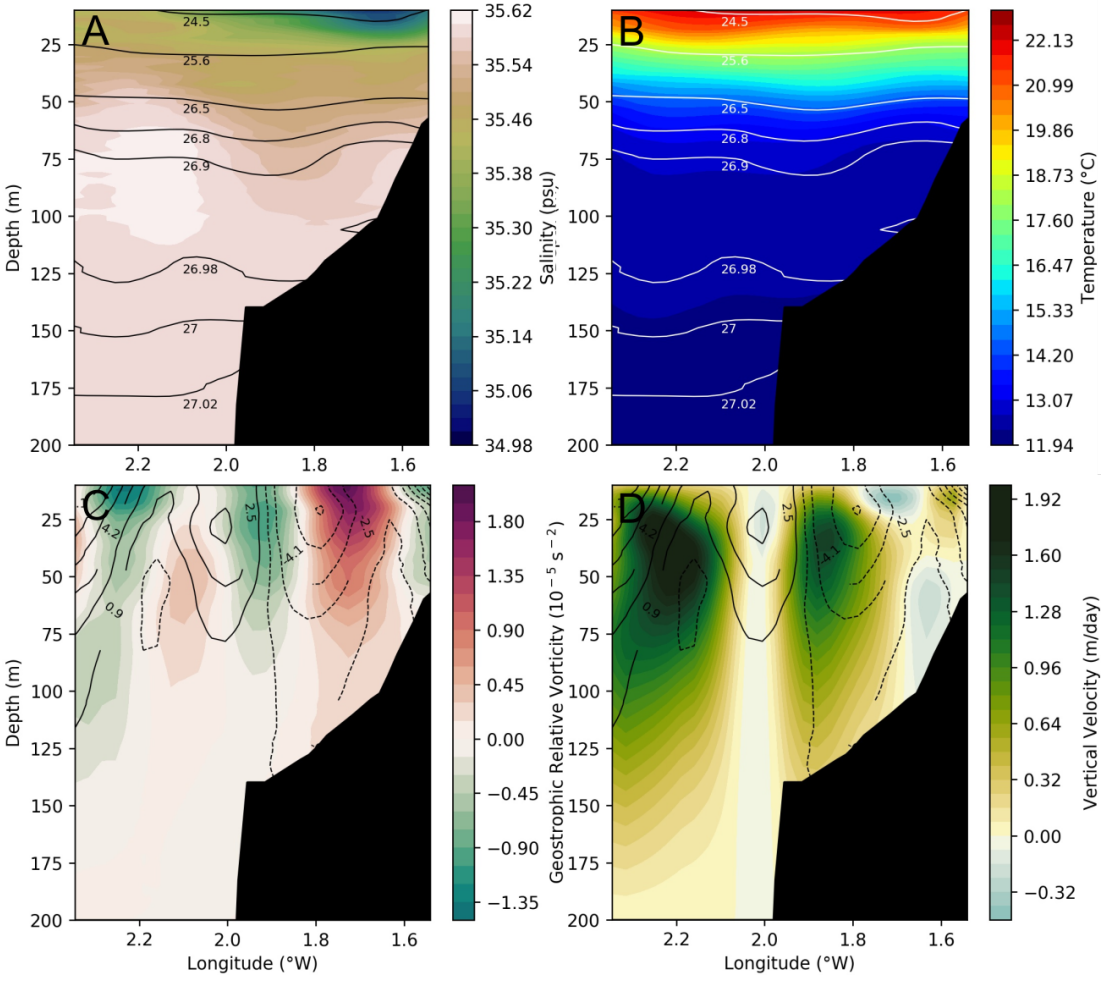

Figure 6. Cross section at 43.77°N (location marked by dashed lines in Figure 5 and 2), representing salinity (A), temperature (B) with isolines (black contours), vorticity (C) and vertical velocities (D) with meridional geostrophic velocities (black contours). Negative (positive) vorticity values represents anticyclonic (cyclonic) circulation. Positive (negative) values for geostrophic velocity represent northward (southward) current.

https://doi.org/10.5194/os-2020-58
Preprint. Discussion started: 18 June 2020

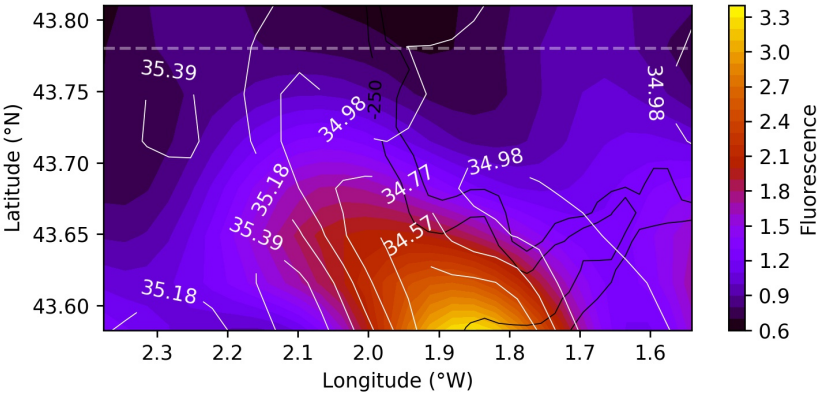

Figure 7. Surface fluorescence recorded by continuous measurements at 3.5 m, white contours represent the salinity field while the black the continental shelf.

https://doi.org/10.5194/os-2020-58
Preprint. Discussion started: 18 June 2020

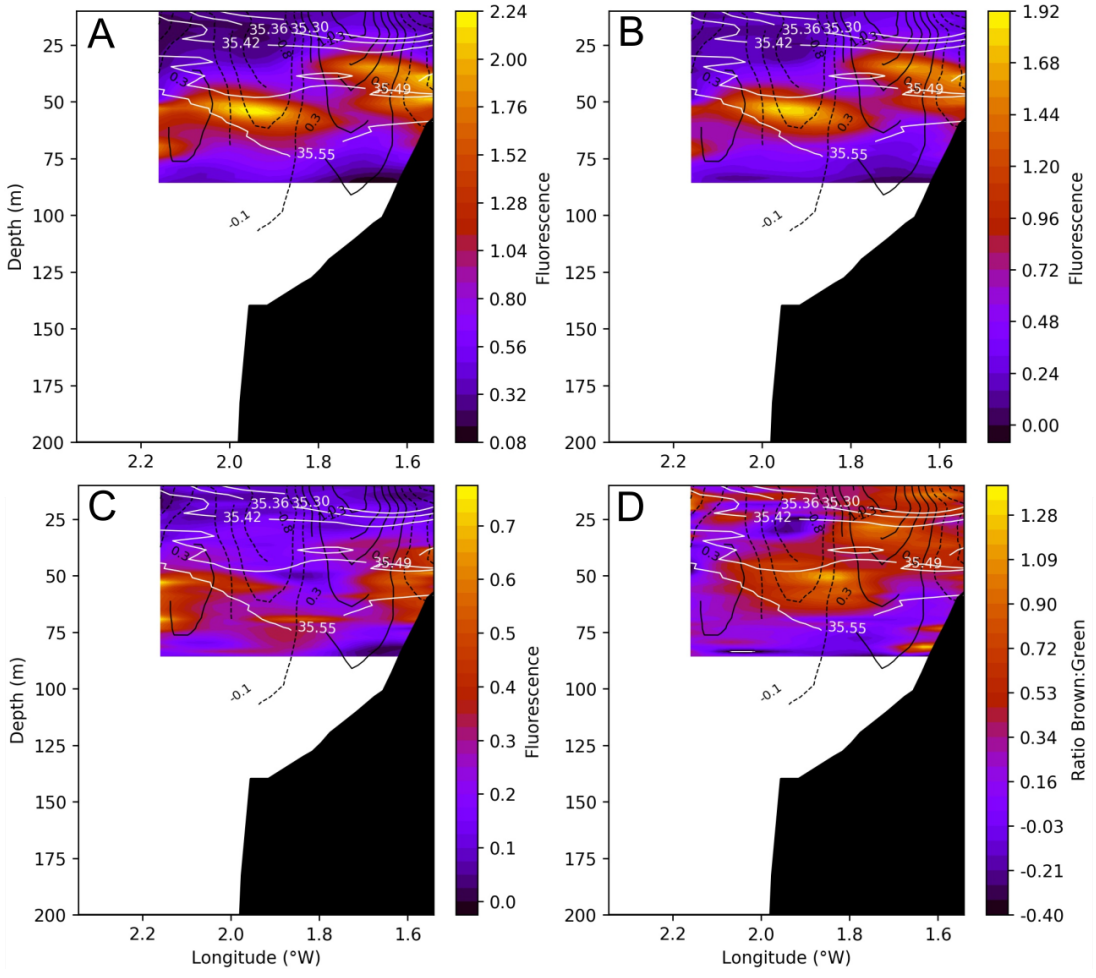

Figure 8. Cross section at 43.77°N of total fluorescence(A), brown algae (B), green algae (C) and the brown:green ratio logarithmically normalized (D). White lines represent salinity contours and black solid (dashed) lines represent positive (negative) vorticity values.

https://doi.org/10.5194/os-2020-58
Preprint. Discussion started: 18 June 2020

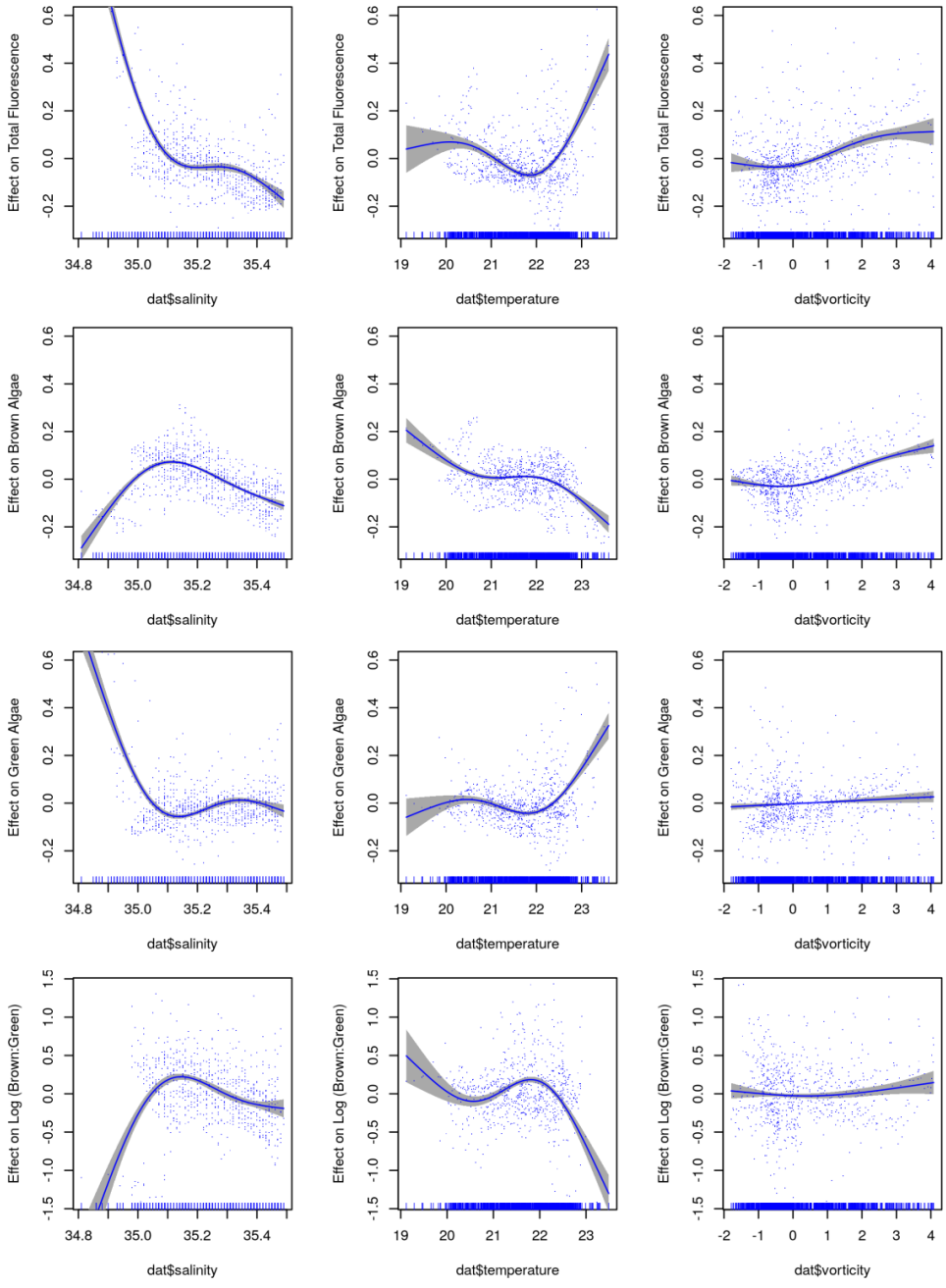

Figure 9. General Additive Model (GAM) for the section above the pycnocline. From top to bottom: Total fluorescence, brown algae, green algae and the brown:green ratio. Shaded area represents the confidence interval of 95%. Non-significant correlations are marked by (*).

https://doi.org/10.5194/os-2020-58
Preprint. Discussion started: 18 June 2020

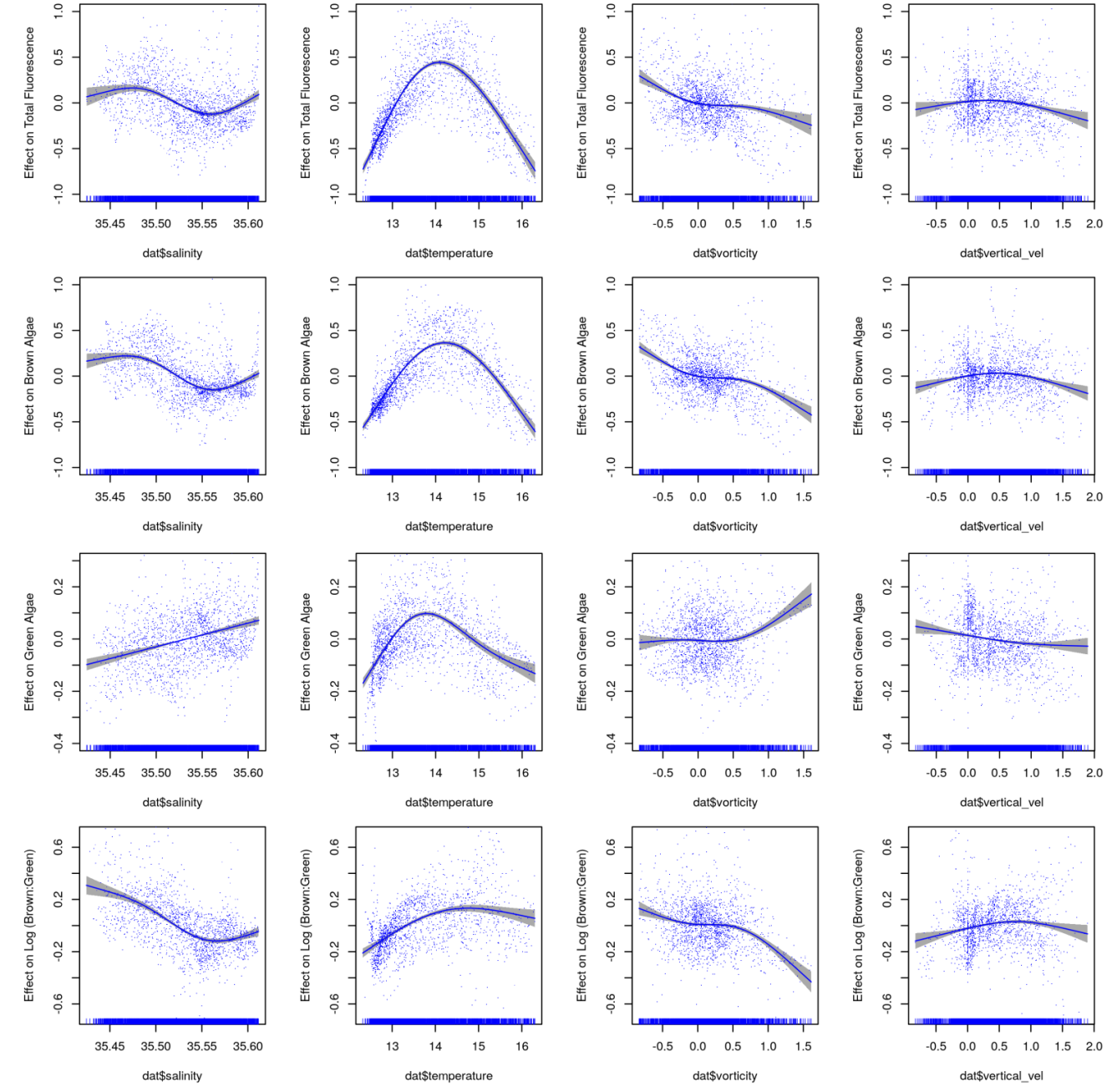

Figure 10. General Additive Model (GAM) for the section below the pycnocline. From top to bottom: Total fluorescence, brown algae, green algae and the brown:green ratio. Shaded area represents the confidence interval of 95%.

https://doi.org/10.5194/os-2020-58
Preprint. Discussion started: 18 June 2020

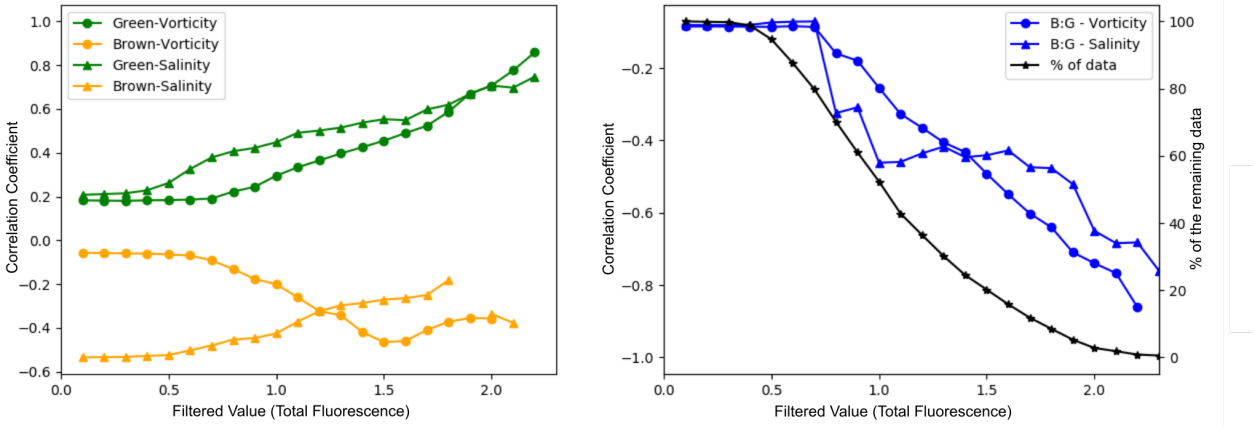

Figure 11. Iterative correlations for brown and green algae (left) and brown:green ratio as well as the percentage of remaining data (right). Only significant correlation are plotted (p-value<0.05).

https://doi.org/10.5194/os-2020-58
Preprint. Discussion started: 18 June 2020

Ocean Science
Discussions
Open Access
EGU

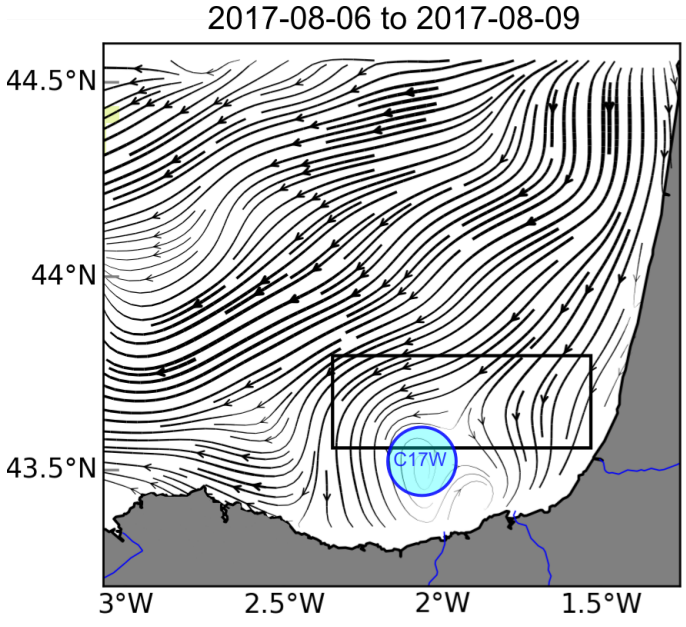

Figure A1. LRC for the period of August 6^{th} to 9^{th}, the persistent C17W eddy is still visible after the change in wind regime.

https://doi.org/10.5194/os-2020-58
Preprint. Discussion started: 18 June 2020

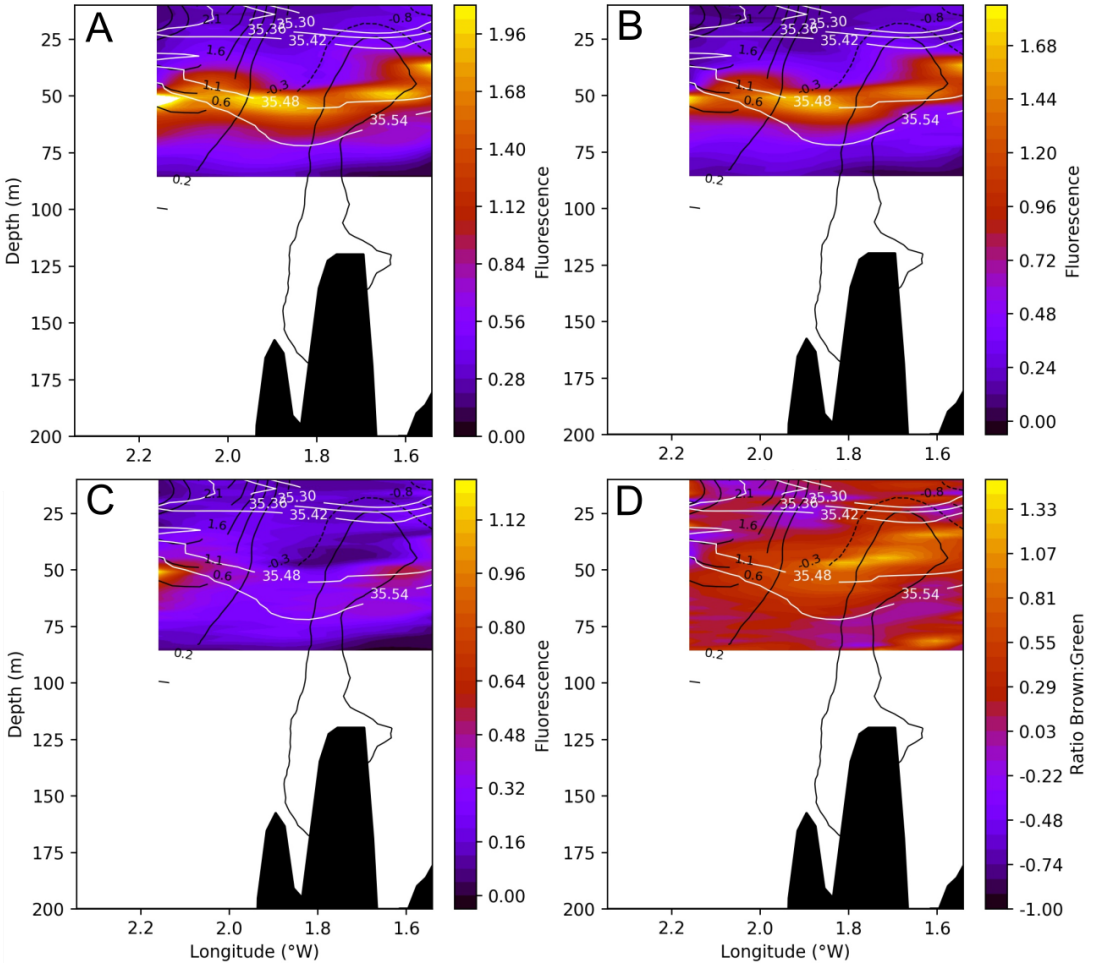

Figure A2. Cross section at 43.70°N of total fluorescence(A), brown algae (B), green algae (C) and the brown:green ratio (D). White lines represent salinity contours and black solid (dashed) lines represent positive (negative) vorticity values.